


Article

Discrete Heaped Model of Tobacco Strips Drying and Characteristics Analysis of Heat and Mass Transfer

Qiike Wei , Lihua Wang *, Wei Jiang, Huaiyu Wang and Hao Zhang

Faculty of Mechanical and Electrical Engineering, Kunming University of Science and Technology, Kunming 650500, China

* Correspondence: wanglihua@kust.edu.cn

Abstract: To accurately study the drying characteristics of tobacco strips in the process of redrying, a discrete heaped physical model of tobacco strips is built. Based on this model, a convective drying multiphase porous media model of the heaped tobacco strips is established, which considers the binary diffusion and transport of vapor inside and outside the tobacco leaf. The model is solved using COMSOL Multiphysics, and the accuracy of the model is verified by experiments. The changes in hot air velocity, vapor and moisture content, and evaporation rate in heaped tobacco strips with different thicknesses are analyzed. The results show that: it is feasible to study the drying characteristics of tobacco strips in redrying using a discrete heaped model; there were significant differences in water content, evaporation rate, and temperature in different regions of heaped tobacco strips; the increase in heaping thickness will significantly reduce the uniformity of heat and mass transfer of tobacco strips in the process of convection drying. This model can provide a reference for the study of heat and mass transfer in porous media, such as tobacco strips in the heaping state.

Keywords: tobacco redrying; discrete heap; drying model; porous media; heat and mass transfer



Citation: Wei, Q.; Wang, L.; Jiang, W.; Wang, H.; Zhang, H. Discrete Heaped Model of Tobacco Strips Drying and Characteristics Analysis of Heat and Mass Transfer. *Energies* **2022**, *15*, 8428. <https://doi.org/10.3390/en15228428>

Academic Editor: Andrea Frazzica

Received: 15 October 2022

Accepted: 7 November 2022

Published: 10 November 2022

Publisher's Note: MDPI stays neutral with regard to jurisdictional claims in published maps and institutional affiliations.



Copyright: © 2022 by the authors. Licensee MDPI, Basel, Switzerland. This article is an open access article distributed under the terms and conditions of the Creative Commons Attribution (CC BY) license (<https://creativecommons.org/licenses/by/4.0/>).

1. Introduction

Redrying is an important link in the tobacco production process [1,2] and has an important influence on improving the quality and long-term storage of tobacco [3,4]. Tobacco redrying is generally performed by hot air convection [5–7], which is a complex multi-physical process coupled with temperature and moisture transport. Establishing a reliable mathematical model of drying can accurately simulate the redrying process of tobacco strips [8–10], reveal the internal heat and mass transfer characteristics of heaped tobacco strips, and then realize the parameter optimization of related processes [11,12].

At present, in the study of tobacco drying, Zhang et al. [13] developed a tobacco moisture migration model using Fick's second law and studied the effects of different temperature and humidity conditions on tobacco drying characteristics. Huang et al. [14] analyzed the humidification and drying characteristics of tobacco strips by combining water migration rate, kinetic model, and parameter applicability. Bai et al. [15] developed a computational fluid dynamics model for tobacco leaf drying using the $k-\epsilon$ turbulence model and discrete phase model and analyzed the effects of bulk tobacco density and thickness on the temperature field and humidity field in drying oven. Guo et al. [5] proposed a method combining thermogravimetric analysis and online nuclear magnetic resonance analysis to study the changes in water flow and distribution in tobacco leaves during drying. Zhu et al. [16] developed a mathematical model, describing the heat and mass transfer of tobacco, which was used to simulate the temperature and moisture evolution of tobacco during two-stage drying. Xin et al. [17] proposed a modified Arrhenius-type equation of diffusivity to describe the influence of temperature and relative humidity on the drying characteristics of tobacco strips and obtained a thin-layer drying model suitable for tobacco leaves through experiments.

In other drying fields, Zhu et al. [18] established a multiphase porous media model of thermo-hydro-mechanical bidirectional coupling for mushroom. Researchers observed the hysteresis movement of the area with high evaporation rate to the internal area of mushroom and analyzed the influence of shrinkage deformation on mushroom drying. Kumar et al. [19] established a multiphase porous media model for apples and studied the transport modes of water and gas in porous media and the relative contribution of phase transition. Bezerra et al. [20] evaluated the mass transfer characteristics of passion fruit peel during convective drying using an analytical model and described the moisture diffusion coefficients via use of the Arrhenius approximate equation. Wei et al. [21] developed three-dimensional (3D) body-fitted geometric models of single-component and multi-component corn kernels with actual structure sizes, analyzing the evolution of internal temperature and moisture content of corn kernels during drying. Shen et al. [22] studied the drying characteristics of germinated brown rice by continuous microwave drying in the process of mobile drying. In conclusion, in the existing studies on convective drying, research subjects are regarded as a single multiphase porous medium and studies on discrete heaped porous media model combining multiphase porous media models of convection drying with heaping materials are rare.

In this study, a discrete heaped physical model of tobacco strips is built, and a convective drying multiphase porous media model of heaped tobacco strips in the redrying process is established further. The accuracy of this model is verified by experiments. The specific objectives of this paper are as follows:

- (1) To investigate the effects of heaping thickness on drying air velocity, moisture content, temperature, and evaporation rate of heaped tobacco strips in the process of redrying.
- (2) To obtain the heat and mass transfer characteristics of heaped tobacco strips and to provide a theoretical basis for optimizing the redrying process of tobacco.

2. Discrete Heaped Physical Model and Governing Equation

2.1. Discrete Heaped Physical Model of Tobacco Strips

The tobacco strips in the redrying process are divided into five categories according to their maximum size. The sizes and proportions of each type of tobacco strip are shown in Table 1 [2], and the thickness of each tobacco strip is 0.2 mm (measured). Five different-sized tobacco strips were randomly selected as prototypes with which to build tobacco strip models. The contour information of the five kinds of tobacco strips is extracted by MATLAB program. The smooth and closed tobacco strip contour is obtained by fitting contour information with the interpolation curve, and the curvature of the tobacco strip models is realized by using the parametric surface modeling method. Real tobacco strips and corresponding models are shown in Figure 1.

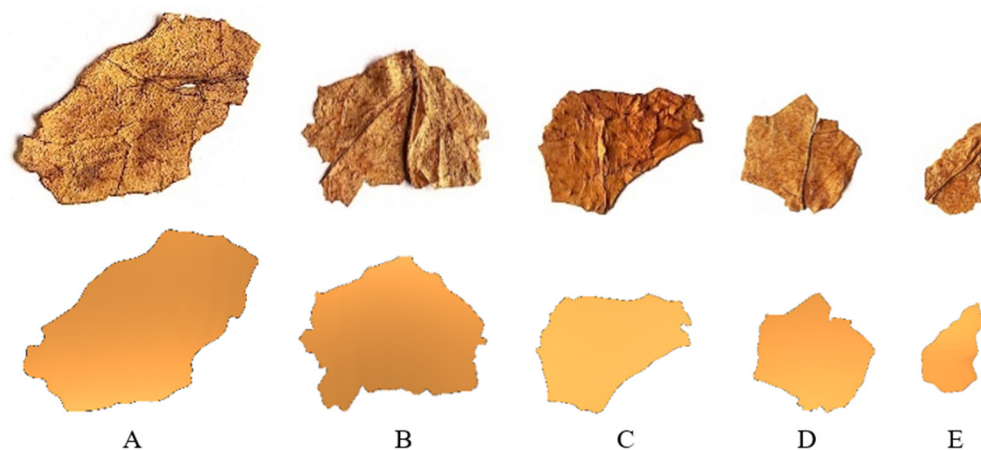


Figure 1. Real tobacco strips and corresponding models.

Table 1. Sizes and proportions of tobacco strips.

Category	Category Code	Size (mm)	Proportion
Large-size tobacco strips	A	27	10%
Medium-size tobacco strips I	B	23	30%
Medium-size tobacco strips II	C	20	20%
Medium-size tobacco strips III	D	15	30%
Small-size tobacco strips	E	8	10%

In actual production, the heaping thickness of tobacco strips on the conveyor belt is regulated by the material limiting device, and the thickness of heaped tobacco strips is usually 60–100 mm. To establish a physical model that more closely matches the actual production, the multi-body dynamics software ADAMS is used to build a discrete heaping model of tobacco strips. During the heaping modeling, the tobacco strips mixed according to the proportion in Table 1 fall freely and are heaped in a box of $100 \times 100 \times 100$ mm. The density of tobacco strips is 280 kg/m^3 , and the friction and damping coefficients between tobacco strips are 0.1 and 10, respectively [2]. Finally, three different heaping thicknesses heaped tobacco strips models are obtained: 60 mm thicknesses model (STM), 80 mm thicknesses model (ETM), and 100 mm thicknesses model (HTM). The 3D model of heaped tobacco strips is shown in Figure 2b.

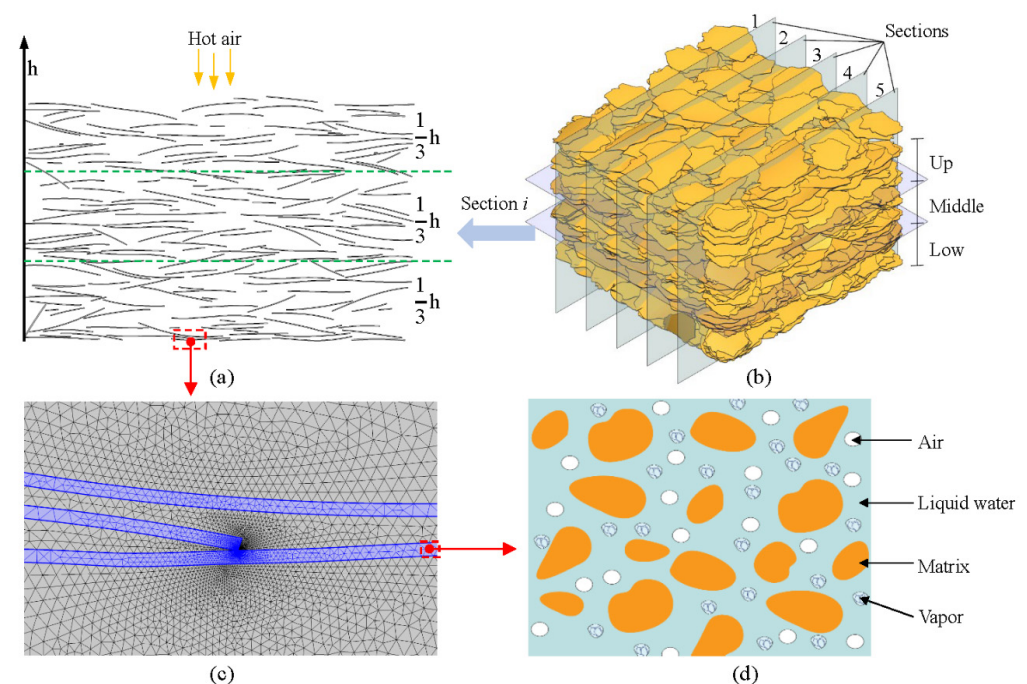


Figure 2. Simplification, grid, and representative elementary volume of heaped tobacco strips model. (a) 2D cross-section of 3D model; (b) 3D model and division principle; (c) grid in contact area; (d) representative elementary volume with different phases.

The thickness of tobacco strips is very small and can be considered a kind of thin layer material. For the 3D heaped model, the contact between tobacco strips leads to plenty of sharp boundaries in the air domain, which greatly reduces the quality of mesh elements and increases the non-convergence in the calculation. To improve the calculation accuracy, more refined mesh elements are needed to ensure the mesh quality during simulation calculation, especially in the contact area between tobacco strips, as shown in Figure 2c. However, the finer elements have extremely high configuration requirements on the computer, which greatly increases the computational cost (if the quality of the grid is to be greater than 0.1, the 3D STM will generate more than 40 million elements). To solve this problem, five two-dimensional (2D) sections perpendicular to the thickness direction are cut equidistantly

on the 3D model, as shown in Figure 2b. For the analysis of the results, the average value of the five sections is taken to obtain the drying characteristics of heaped tobacco strips. This method not only greatly reduces the calculation cost, but also considers the influence of the spatial position of heaped tobacco strips on drying. In addition, for the purpose of analyzing the drying uniformity of heaped tobacco strips, it is divided into upper, middle, and lower parts, as shown in Figure 2a,b.

2.2. Governing Equation

Figure 2 depicts the simplifications of the heaped tobacco strips model from three-dimension to two-dimension, the grid in the contact area, and all phases of the porous media domain. Heat and mass transfer take place at all boundaries of 2D sections of heaped tobacco strips. Tobacco strips are considered porous media, and the pores are filled with three transportable phases (liquid water, air and vapor). All phases (solid matrix, liquid water, air, and vapor) are continuous, and local thermal equilibrium is available. Liquid water transport occurred due to the gas pressure gradient, capillary flow, and evaporation. Vapor and air transport results from gas pressure gradients and binary diffusion. Convective drying of the tobacco strips is a multi-physical problem coupling fluid flow, heat, and mass transfer. The governing equations of the mathematical model include a fluid flow equation, a mass equation, and an energy equation, which are based on the following assumptions:

- (1) Tobacco strips are regarded as isotropic non-saturated multiphase porous media, which consist of solid matrix, liquid water, air, and vapor.
- (2) All phases in the tobacco strips are continuous and local thermal equilibrium.
- (3) The effects of gravity and shrinkage of tobacco strips cross-section during drying are ignored.

2.2.1. Flow Conditions

According to the actual processing, the velocity of hot air is 1.5 m/s. The Reynolds number is about 10,000 (characteristic length is 0.1 m), which means that the flow in the drying oven is turbulence flow [23]. The heat and mass transfer process in convection drying is usually controlled by external turbulent conditions, so the standard Reynolds-Averaged Navier–Stokes (RANS) equation is adopted. In addition, k - ϵ model is selected to describe the external flow field. The transfer of the turbulent kinetic energy (k) and transfer of the turbulent energy dissipation rate (ϵ) are expressed by Equations (1) and (2), respectively:

$$\frac{\partial(\rho_g k)}{\partial t} + \nabla \cdot (\rho_g \vec{u} k) = \nabla \cdot \left[\left(\mu_g + \rho_g C_\mu \frac{k^2}{\epsilon \sigma_k} \right) \nabla k \right] + P_k - \rho_g \epsilon \quad (1)$$

$$\frac{\partial(\rho_g \epsilon)}{\partial t} + \nabla \cdot (\rho_g \vec{u} \epsilon) = \nabla \cdot \left[\left(\mu_g + \rho_g C_\mu \frac{k^2}{\epsilon \sigma_\epsilon} \right) \nabla \epsilon \right] + C_{\epsilon 1} \frac{\epsilon}{k} P_k - C_{\epsilon 2} \rho_g \frac{\epsilon^2}{k} \quad (2)$$

where, u is the velocity field of hot air and P_k is the turbulent energy source term [$\text{N} \cdot \text{m}^{-2} \text{s}^{-1}$]. C_μ , $C_{\epsilon 1}$ and $C_{\epsilon 2}$ are model constants. σ_k and σ_ϵ are diffusion and dissipation of turbulent kinetic energy: in this study, their values are 0.09, 1.44, 1.92, 1.0, and 1.3, respectively [24].

2.2.2. Mass Equation

The representative elementary volume (ΔV) is defined as the sum of the three-phases volumes (gas, water, and solid), expressed as:

$$\Delta V = \Delta V_g + \Delta V_w + \Delta V_s \quad (3)$$

where, ΔV_g is the volume of gas phase (including air and vapor, m^3), ΔV_w and ΔV_s are the volumes of water and solid phase [m^3], respectively.

The porosity φ is defined as the volume fraction of gas and water phase in the representative elementary volume:

$$\varphi = \frac{\Delta V_g + \Delta V_w}{\Delta V} \quad (4)$$

The water saturation S_w and gas saturation S_g are defined as the fraction of that particular phase in pore volume.

$$S_w = \frac{\Delta V_w}{\Delta V_w + \Delta V_g} = \frac{\Delta V_w}{\varphi \Delta V} \quad (5)$$

$$S_g = \frac{\Delta V_g}{\Delta V_w + \Delta V_g} = \frac{\Delta V_g}{\varphi \Delta V} = 1 - S_w \quad (6)$$

The mass concentrations of water (c_w , $\text{kg} \cdot \text{m}^{-3}$), vapor (c_v , $\text{kg} \cdot \text{m}^{-3}$), and air (c_a , $\text{kg} \cdot \text{m}^{-3}$) can be expressed by the following formulas, respectively:

$$c_w = \rho_w \varphi S_w \quad (7)$$

$$c_v = \frac{p_v M_v}{R_{\text{const}} T} \varphi S_v \quad (8)$$

$$c_a = \frac{p_a M_a}{R_{\text{const}} T} \varphi S_a \quad (9)$$

where, R_{const} is the universal gas constant [$\text{J} \cdot \text{mol}^{-1} \text{K}^{-1}$], ρ_w is the density of water [$\text{kg} \cdot \text{m}^{-3}$], P_v is the partial pressure of vapor [Pa], P_a is the partial pressure of air [Pa], M_a and M_v are molar masses of air and vapor [$\text{kg} \cdot \text{mol}^{-1}$], respectively.

Dry basis moisture content M_d represents the water mass contained in the solid matrix per unit mass:

$$M_d = \frac{c_w + c_v}{(1 - \varphi) \rho_s} \quad (10)$$

The mass transfer of tobacco strips during convective drying is related to water and vapor, and the transfer of liquid water only occurs in the porous media. Because of the evaporation, a mass source term is generated in the mass equation of liquid water:

$$\frac{\partial}{\partial t}(\varphi S_w \rho_w) + \nabla \cdot (\vec{n}_w) = -R_{\text{evap}} \quad (11)$$

where, \vec{n}_w is the mass flux of water ($\text{kg} \cdot \text{m}^{-2} \text{s}^{-1}$), given by

$$\vec{n}_w = -\rho_w \frac{k_{i,w} k_{r,w}}{\mu_w} \nabla P - D_{\text{cap}} \nabla c_w \quad (12)$$

Here, P is the total gas pressure [Pa], $\kappa_{i,w}$ is the intrinsic permeability of water [m^2], and $\kappa_{r,w}$ is the relative permeability of water. The dynamic viscosity of water μ_w [$\text{Pa} \cdot \text{s}$] is a function of temperature [25], and the capillary diffusivity D_{cap} is a function of M_d [26]. The first term in Equation (12) is the mass flux of water due to the gradient of gas phase pressure by Darcy's law. The second term is capillary diffusivity caused by the concentration gradient, which represents the mass flux of water due to capillary pressure. In Equation (12), the capillary diffusivity due to temperature gradient (Soret effect) is omitted because its effect is not significant compared with the capillary diffusivity caused by the concentration gradient [25].

The mass equation for vapor is described in two parts. One part is the vapor in the drying oven, given by:

$$\frac{\partial}{\partial t}(\varphi S_g \rho_g \omega_v) + \nabla \cdot (\vec{n}_{\text{amb},v}) = 0 \quad (13)$$

where, ρ_g is gas density related to the molar fraction of air and vapor [27]. The mass flux of vapor $\vec{n}_{amb,v}$ in the drying oven is determined by hot air flow and the binary diffusivity D_{va} of vapor in air [25].

$$\vec{n}_{amb,v} = -\vec{u}\rho_v - D_{va}\nabla c_v \quad (14)$$

The other part is the vapor generated by the evaporation of water inside the porous media, and there is a mass source term in the mass equation. The vapor mass equation in a porous media can be expressed as:

$$\frac{\partial}{\partial t}(\phi S_g \rho_g \omega_v) + \nabla \cdot (\vec{n}_v) = R_{evap} \quad (15)$$

where, \vec{n}_v is the mass flux of vapor [$\text{kg}\cdot\text{m}^{-2}\text{s}^{-1}$] in porous media area, given by:

$$\vec{n}_v = -\rho_g \omega_v \frac{k_g k_{r,g}}{\mu_g} \nabla P - \phi S_g \rho_g D_{eff,g} \nabla \omega_v \quad (16)$$

Here, $\kappa_{r,g}$ and $\kappa_{r,g}$ are the intrinsic permeability and the relative permeability of gas [m^2], respectively. The dynamic viscosity of the gas phase μ_g [$\text{Pa}\cdot\text{s}$] is related to the mole fraction of vapor and air [27]. The effective diffusivity of vapor and air $D_{eff,g}$ [$\text{m}^2\cdot\text{s}^{-1}$] is a function of porosity and saturation of the gas [26].

The mass equation for the gas phase is given by:

$$\frac{\partial}{\partial t}(\phi S_g \rho_g) + \nabla \cdot (\vec{n}_g) = R_{evap} \quad (17)$$

where, the mass flux of gas n_g can be expressed as:

$$\vec{n}_g = -\rho_g \frac{k_g k_{r,g}}{\mu_g} \nabla P \quad (18)$$

Usually, the vapor pressure and equilibrium pressure are not equal in porous media during drying. Therefore, the non-equilibrium theory is used to describe the evaporation rate R_{evap} [$\text{kg}\cdot\text{m}^{-3}\text{s}^{-1}$] [28].

$$R_{evap} = K_{evap} \frac{M_v}{R_{const} T} (a_w p_{v,sat} - p_v) \phi S_g \quad (19)$$

where, the evaporation constant K_{evap} is defined as the transition of molecules from liquid water to vapor, which depends on the material and process. The water activity a_w and saturated vapor pressure $p_{v,sat}$ are expressed according to references [18,29], respectively.

2.2.3. Energy Equation

According to the assumption of local thermal equilibrium, the temperature of all phases (solid, water, vapor and air) in REV is the same. Since porous media is a multiphase mixture, the thermodynamic parameters should be expressed by effective value [30]. Assumed the properties of the mixture are the average of all pure phases, and thus the effective thermal density ρ_{eff} [$\text{kg}\cdot\text{m}^{-3}$], the effective thermal conductivity k_{eff} [$\text{W}\cdot\text{m}^{-1}\text{K}^{-1}$], and the effective heat capacity $c_{p,eff}$ [$\text{J}\cdot\text{kg}^{-1}\text{K}^{-1}$] are weighted averages of the volume fraction or mass fraction of each phase. They are calculated by:

$$\rho_{eff} c_{p,eff} \frac{\partial T}{\partial t} + \nabla \cdot (\vec{n}_w c_{p,w} + \rho_g \vec{n}_g (\omega_v c_{p,v} + \omega_a c_{p,a})) T = \nabla \cdot (\lambda_{eff} \nabla T) - h_{la} R_{evap} \quad (20)$$

$$\rho_{eff} = c_s + \phi S_w \rho_w + \phi S_g \rho_g \quad (21)$$

$$\lambda_{eff} = \frac{c_s}{\rho_s} \lambda_s + \phi S_w \lambda_w + \phi S_g (\omega_v \lambda_v + \omega_a \lambda_a) \quad (22)$$

$$c_{p,eff} = m_g(\omega_v c_{p,v} + \omega_a c_{p,a}) + m_w c_{p,w} + m_s c_{p,s} \quad (23)$$

2.2.4. Initial and Boundary Conditions

At the initial moment, there is no hot air flow in the drying oven, and the porous media is under the ambient temperature and pressure: $T_{(t=0)} = T_{amb}$, $P_{(t=0)} = P_{amb}$. Meanwhile, the initial mass fraction of vapor in the gas phase $\omega_{v,0}$ is 0.02, and the initial water saturation $S_{w,0}$ is 0.076. The initial value of water mass concentration $c_{w,0}$ can be calculated by Equation (8).

Because all the boundaries of the porous media are completely exposed to the environment during drying, the surface pressure is equal to the ambient pressure. The pressure boundary condition of Equation (18) is $P_{surf} = P_{amb}$. The mass flux of vapor on the surface comes from the evaporation and vapor already present at the surface. Assuming the volume fraction is equal to the surface area fraction, the total vapor flux at boundary is given by:

$$\vec{n}_{v,surf} = h_m \varphi (\rho_{g,surf} \omega_{v,surf} - \rho_{v,amb}) \quad (24)$$

The boundary condition of energy equation includes the transitions of energy caused by convective heat transfer and evaporation [31], and can be expressed as:

$$q_{surf} = h_T (T_{amb} - T_{surf}) + h_m \varphi (\rho_{g,surf} \omega_{v,surf} - \rho_{v,amb}) h_{lv} \quad (25)$$

where, h_T is the heat transfer coefficient and h_m is the mass transfer coefficient. According to reference [31], the heat and mass transfer coefficients are calculated as $h_T = 14.925 \text{ W/m}^2 \text{ K}^{-1}$, and $h_m = 0.014369 \text{ m/s}$, respectively.

2.2.5. Input Parameters

The constant parameters required for solving the mathematical model are shown in Table 2.

Table 2. Constant parameters.

Parameter	Value
Ambient pressure, P_{amb}	101,325 Pa [25]
Ambient temperature, T_{amb}	298.15 K
Temperature, T	333.15 K
Initial velocity, u_0	0 m·s ⁻¹
Inlet velocity, u	1.5 m·s ⁻¹
Binary diffusivity, D_{va}	$2.6 \times 10^{-5} \text{ m}^2 \cdot \text{s}^{-1}$ [25]
Latent heat of evaporation, h_{la}	$2425 \times 10^3 \text{ J} \cdot \text{kg}^{-1}$ [31]
Evaporation constant, K_{evap}	1000 s ⁻¹ [28]
Initial water saturation, $S_{w,0}$	0.076
Irreducible water saturation, $S_{w,ir}$	0.023
Universal gas constant, R_{const}	$8.314 \text{ J} \cdot \text{mol}^{-1} \text{ K}^{-1}$ [32]
Intrinsic permeability of water, $\kappa_{i,w}$	$2.18 \times 10^{-14} \text{ m}^2$
Intrinsic permeability of gas, $\kappa_{i,g}$	$1 \times 10^{-14} \text{ m}^2$
Molar mass of air, M_a	$0.02897 \text{ kg} \cdot \text{mol}^{-1}$ [31]
Molar mass of vapor, M_v	$0.018016 \text{ kg} \cdot \text{mol}^{-1}$ [31]
Molar mass of water, M_w	$0.018016 \text{ kg} \cdot \text{mol}^{-1}$ [31]
Heat capacity of air, $c_{p,a}$	$1006 \text{ J} \cdot \text{kg}^{-1} \text{ K}^{-1}$ [31]
Heat capacity of vapor, $c_{p,v}$	$2029 \text{ J} \cdot \text{kg}^{-1} \text{ K}^{-1}$ [31]
Heat capacity of water, $c_{p,w}$	$4182 \text{ J} \cdot \text{kg}^{-1} \text{ K}^{-1}$ [31]
Heat capacity of tobacco, $c_{p,s}$	$1690 \text{ J} \cdot \text{kg}^{-1} \text{ K}^{-1}$ [33]
Thermal conductivity of air, λ_a	$0.025 \text{ W} \cdot \text{m}^{-1} \text{ K}^{-1}$ [31]
Thermal conductivity of vapor, λ_v	$0.0248 \text{ W} \cdot \text{m}^{-1} \text{ K}^{-1}$ [31]
Thermal conductivity of water, λ_w	$0.59 \text{ W} \cdot \text{m}^{-1} \text{ K}^{-1}$ [31]
Thermal conductivity of tobacco, λ_s	$0.26 \text{ W} \cdot \text{m}^{-1} \text{ K}^{-1}$ [33]
Density of air, ρ_a	$1.025 \text{ kg} \cdot \text{m}^{-3}$ [31]
Density of vapor, ρ_v	$0.596 \text{ kg} \cdot \text{m}^{-3}$ [31]
Density of water, ρ_w	$998.2 \text{ kg} \cdot \text{m}^{-3}$ [31]
Density of tobacco, ρ_s	$280 \text{ kg} \cdot \text{m}^{-3}$ [34]
Porosity, φ	0.55 [35]

2.2.6. Numerical Solution

The mathematical model is solved by using COMSOL Multiphysics. All grids of all models are free triangular meshes. To ensure that the results are grid-independent, the grid-independent verification of the two-dimension model of STM is tested three times, and the results are shown in Table 3. The errors of moisture content (dry basis) under three different grids are less than 1% at 60 s, which indicates that the solution is independent of the grid. In this paper, all of the two-dimensional models use the same settings as Grid 1. The maximum element size of all models is 1 mm, and the minimum element quality is 0.2. The time step is 0.1 s, and the simulation time is 180 s.

Table 3. Grid-independent verification ($v = 1.5$ m/s, $T = 60$ °C).

Grid	Element Number	Minimum Element Quality	M_d (t = 60 s)	Relative Error
Grid 1	247,154	0.2187	0.16887	1→3, 0.315%
Grid 2	272,767	0.2069	0.16780	1→2, 0.634%
Grid 3	346,907	0.1984	0.16940	2→3, 0.955%

3. Experiment Method

The raw material for tobacco strips comes from a redrying factory and is stored at an ambient temperature of 25 °C before the experiments. Tobacco strips of five sizes are mixed into a box with the size 100 mm × 100 mm × 100 mm (the box is made of wire mesh and the mesh side length is 10 mm), and the heaping thickness of the sample in the box is approximately 60 mm. The temperature and the inlet velocity of hot air are 60 °C and 1.5 m/s, respectively. After each drying experiment, the sample is heated to 100 °C for at least 2 h to get dry basis mass to calculate the initial moisture content of the sample. The moisture losses are recorded at regular intervals of 15 s with a digital balance (0.0001 g accuracy). Since the differences in samples' mass before each drying experiment, the experiments are completed three times and the average value is calculated.

4. Result and Discussion

4.1. Validation of Mathematical Model

The average moisture content obtained from the experiments and STM are compared in Figure 3. The experimental and simulated results are coincident. The determination coefficient R^2 can be used to determine the goodness of fit of simulation and experiment results: the closer to 1, the higher the goodness of fit. Additionally, the R^2 is found to be larger than 0.98 in this study, which indicates that the discrete heaped porous media model proposed in this paper can accurately describe the convection drying process of heaped tobacco strips.

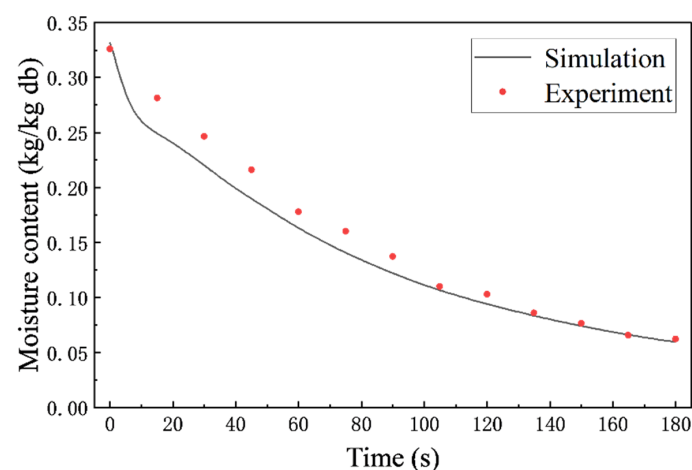


Figure 3. The average dry basis moisture content comparison between experiment and simulation.

4.2. Effect of Heaping Thickness on the Velocity of Hot Air

The variation of the velocity of hot air in the interstices of heaped tobacco strips with different heaping thicknesses with the spatial position is shown in Figure 4. Although the heaping thickness is different, the hot air velocity in the interstices changes in the same trend. One reason for this is that the resistance of air entering the interstices increases and the pressure decreases. Another reason is that the water in the upper region of the heaped tobacco strips starts to evaporate after coming into contact with hot air, and the rise in the vapor concentration in the gas leads to the increase in the dynamic viscosity of the gas. The velocity of hot air in the middle and lower regions of heaped tobacco strips is maintained at a low value and changed little. This indicates that the distribution of hot air velocity in heaped tobacco strips is not uniform. The hot air velocity in the upper region near the air inlet is significantly higher than that in the middle and lower regions. This phenomenon has a great impact on the drying characteristics of the heaped tobacco strips, which is the reason for the uneven heat and mass transfer among different regions in the heap.

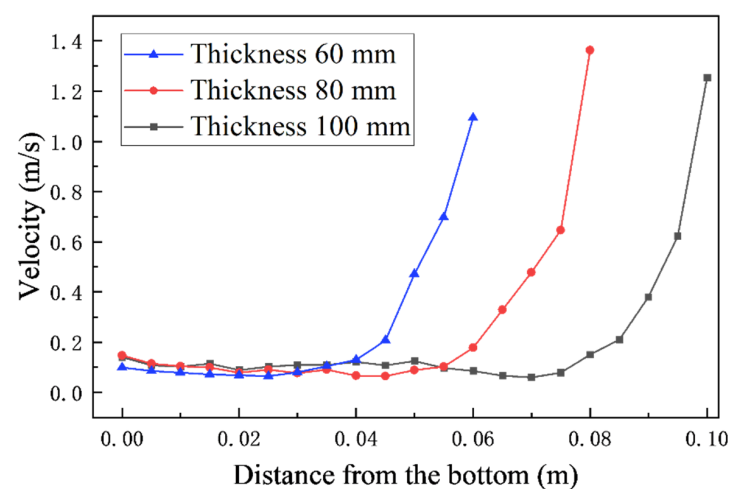


Figure 4. Variation in hot air velocity in heaped tobacco strips.

4.3. Effect of Heaping Thickness on Moisture Content

The variation in dry basis moisture content of heaped tobacco strips in different heaping thickness models is shown in Figure 5. The dry basis moisture content trends of the three models are consistent. At the beginning of drying, the moisture content decreased rapidly. Meanwhile, a trend emerged whereby the thinner the heaping thickness, the more obvious the decrease in water content, and different heaping thicknesses cause a great difference in moisture content. For example, at 60 s, the maximum deviation in the moisture content of three heaping thicknesses reached 28.67%, which indicates that the heaping thickness of tobacco strips has a significant impact on the drying effect.

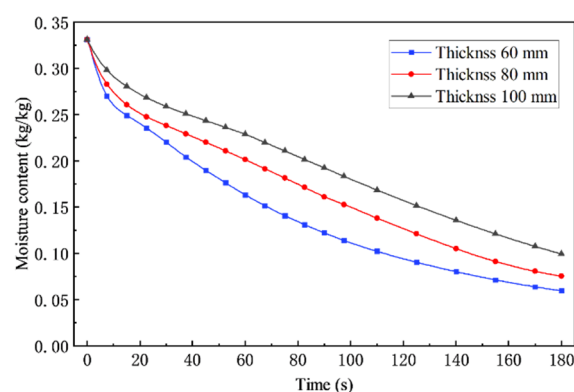


Figure 5. Overall average moisture content of the heaped tobacco strips models.

Figure 6 depicts the variation of dry basis moisture content in the upper, middle, and lower regions of the model with three heaping thicknesses. For the moisture content of tobacco strips in the upper region, although the three models show a consistent change trend, the water content at the same moment varies dramatically. This is because the thickness of the upper region of the STM is only 20 mm, while that of the HTM is about 33 mm. The increase in the thickness reduces the decline rate of the average moisture content, which is consistent with the overall moisture content variation caused by the thickness described in Figure 5. However, the change of moisture content in the middle region is different from that in the upper region. At the beginning of drying, the dry base moisture content in the middle region of the three models showed a small increase, and the rising time is gradually prolonged with the increase in the heaping thickness. This is because the velocity of hot air in the middle region is very low and contains a large amount of vapor evaporated from the upper region, while the temperature in the central region rises more slowly (as will be studied in Section 4.5), and parts of the vapor undergo a phase transition, which leads to a rewetting phenomenon in the middle region.

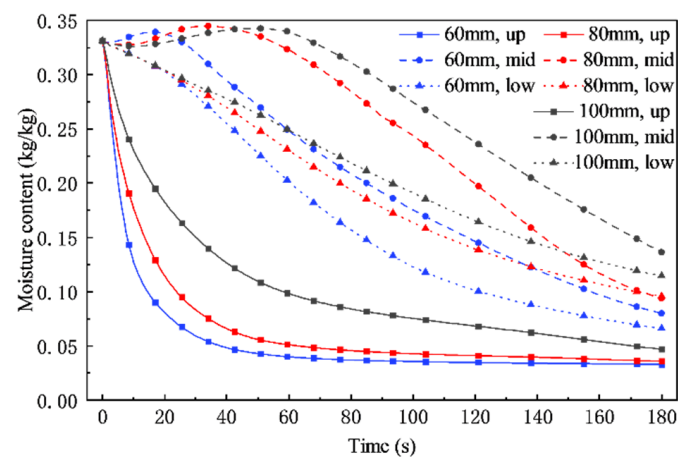


Figure 6. Average moisture content in different regions of the heaped tobacco strips models.

Figure 7 depicts the evolution of vapor concentration in heaped tobacco strips. At the beginning of drying, a large amount of vapor is first generated in the upper region of the heaped tobacco strips. Then, the high concentration vapor is generated in the middle region at 20 s and in the lower region at 50 s. This indicates that high evaporation rate first occurs in the upper region and then gradually transfers to the middle and lower regions. In addition, with the increase in heaping thickness, the non-uniformity of moisture content distribution in heaped tobacco strips is more significant. For example, at 180 s, the maximum deviation of moisture content in the three regions of STM is about 0.047, while that of ETM and HTM are about 0.063 and 0.089, respectively. This further indicates that the heaping thickness of tobacco strips has great influence on the drying effect.

4.4. Effect of Heaping Thickness on Evaporation Rate

The overall evaporation rate of the heaping model is shown in Figure 8. At the beginning of drying, the evaporation rate increases rapidly and reaches a peak, which is related to the temperature of the tobacco leaves. Because the tobacco strips are suddenly exposed to hot air at the beginning, their temperature rises rapidly. Additionally, in the early stage of drying, the average evaporation rate of STM is significantly higher than that of ETM, while the average evaporation rate of HTM is the lowest. This indicates that the heaping thickness of tobacco strips has great influence on the evaporation rate, and that the effect is more significant with the increase in the heaping thickness.

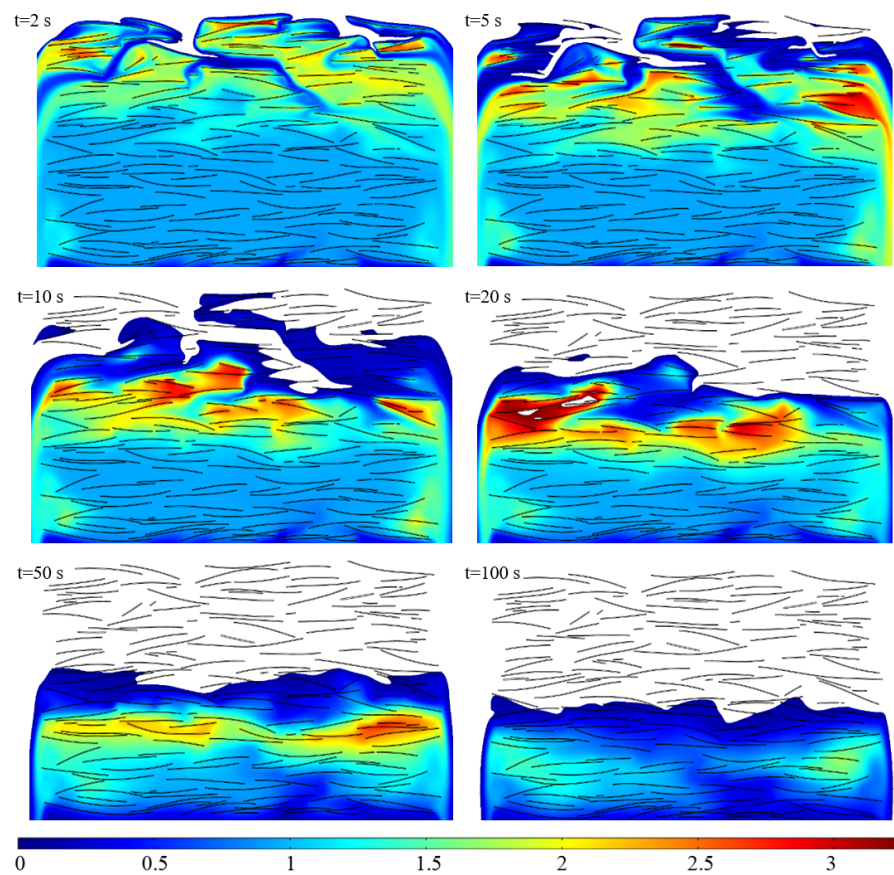


Figure 7. Evolution of vapor concentration in heaped tobacco strips (section *i*, thickness, 60 mm, unit: $\text{mol}\cdot\text{m}^{-3}$).

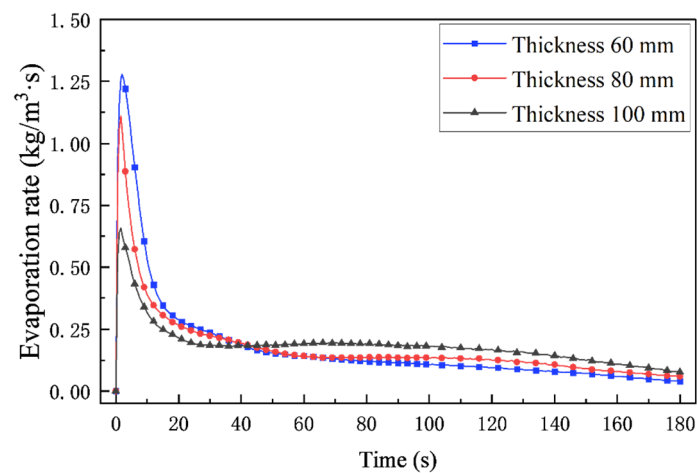


Figure 8. Overall average evaporation rate of the heaped tobacco strips models.

Figure 9 depicts the variation of evaporation rate in the upper, middle, and lower regions of tobacco strips with three heaping thicknesses. The average evaporation rate of the upper part of the three thicknesses is consistent with the overall average evaporation rate, while the average evaporation rate of the lower part is always kept at a low value. At the beginning of drying, the average evaporation rate in the central region decreased to a negative value, then gradually increased to a positive value, and finally approached zero. Additionally, in the later drying stage (after about 60 s), the thicker the accumulation thickness, the higher the evaporation rate in the middle region. In conclusion, the upper region is the main factor affecting the overall evaporation rate in the early drying stage; in the later drying stage, the middle region has a more significant impact on the overall

rate. In addition, at the early stage of drying, the evaporation rate in the central region decreases to a negative value because tobacco strips absorb part of the water vapor in the air (according to the analysis in Section 4.3), and the saturated vapor pressure in tobacco leaf pores decreases so that $R_{evap} < 0$ in Equation (19).

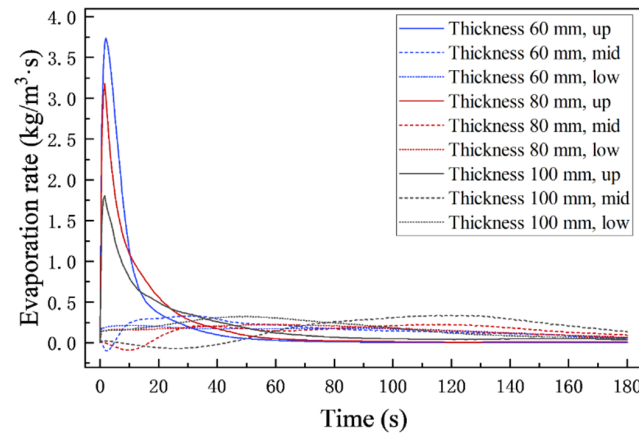


Figure 9. Average evaporation in different regions of the heaped tobacco strips models.

4.5. Effect of Heaping Thickness on Temperature

Figures 10 and 11 show the temperature changes in the overall and each region of the heaped tobacco model with different thicknesses, respectively. At the beginning of drying, the temperature of tobacco strips rises sharply: this is because the tobacco strips are suddenly exposed to hot air, and the heat is transferred to the outer region of heaped tobacco strips through convection. Then, the heat is gradually transferred to the interior region of the heap. Because the evaporation of water in the tobacco strips absorbs a large amount of heat, the temperature rises slowly. As drying continues, the evaporation rate declines, and the heat absorbed by evaporation gradually decreases. Therefore, the temperature of tobacco strips slowly approaches the drying temperature. With the increase in the heaping thickness, the temperature rise rate of each region decreases significantly, which is finally reflected in the overall temperature change. In addition, the average temperature of the upper region increased the fastest, while that of the lower region increased the slowest, this is because hot air flows in from above, and the convective heat transfer occurs in the upper region first. Furthermore, the increase in the heaping thickness also aggravates the temperature differences in the three regions. For example, at 180 s, the maximum temperature deviation of the three regions of STM is about 0.7 °C, while that of ETM is about 8.7 °C. In short, the increase in heaping thickness will significantly slow down the overall temperature rise rate, and also aggravates the uneven heat transfer in heaped tobacco strips.

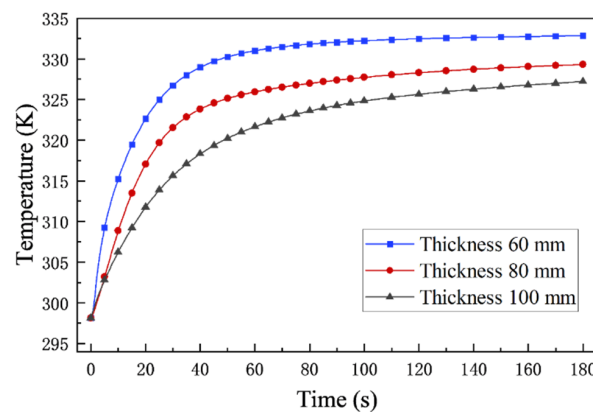


Figure 10. Overall average temperature of the heaped tobacco strips models.

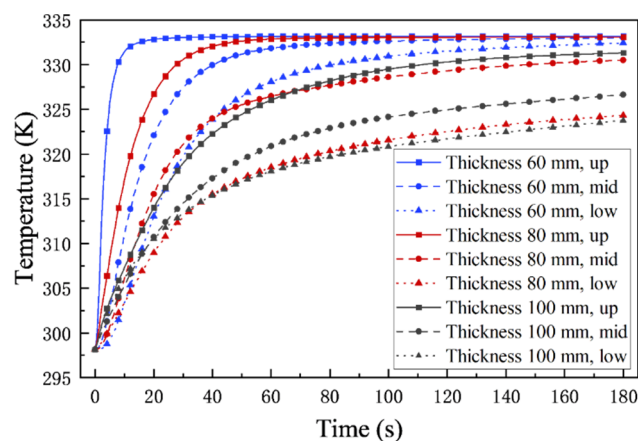


Figure 11. Average temperature in different regions of the heaped tobacco strips models.

5. Conclusions

In this paper, to study the effect of heaping thickness on heat and mass transfer during convection drying of tobacco strips, a discrete heaped model of tobacco strips in the stage of tobacco redrying is established. Additionally, based on this model, a multiphase porous media model for convection drying of tobacco strips is established. The feasibility of the model is verified by experiments, and the heat and mass transfer characteristics of heaped tobacco strips during convection drying are studied comprehensively. The main conclusions are as follows:

1. In the convective drying process, the heaping thickness has a great influence on the moisture content of tobacco strips. The velocity of hot air decreased rapidly after entering the upper region of heaped tobacco strips, and the high evaporation rate region also transfers from the top to bottom. At the same moment, with the increase in heaping thickness, the deviation of the overall moisture content of the tobacco strips increases, and the moisture content uniformity of the tobacco strips also becomes worse.
2. The heaping thickness of tobacco strips has a great influence on the evaporation rate. The increase in the heaping thickness reduces the peak value of the overall evaporation rate. The overall evaporation rate change is mainly related to the upper region of the heaped tobacco strips at the early stage of drying, while the influence mainly comes from the middle region of the heaped tobacco at the middle and late stages of drying.
3. The temperature variation of tobacco strips is also greatly affected by the heaping thickness. With the increase in heaping thickness, the overall temperature of heaped tobacco strips decreased significantly, and the temperature difference of tobacco strips in different regions increased, all of which reduce the uniformity of tobacco drying.

Author Contributions: Conceptualization, Q.W. and L.W.; methodology, Q.W., L.W. and W.J.; software, Q.W., H.W. and W.J.; validation, Q.W., W.J., H.W. and H.Z.; formal analysis, Q.W., W.J. and H.Z.; investigation, Q.W.; resources, L.W. and Q.W.; data curation, Q.W.; writing—original draft preparation, Q.W.; writing—review and editing, L.W. and W.J.; supervision, L.W.; project administration; funding acquisition, L.W. All authors have read and agreed to the published version of the manuscript.

Funding: This research is funded by Major Science and Technology Special Project of Yunnan Province of China, grant number 202002AD080001.

Data Availability Statement: Not applicable.

Acknowledgments: Thanks for the financial support of Major Science and Technology Special Project of Yunnan Province of China Fund for this research.

Conflicts of Interest: The authors declare no conflict of interest.

Nomenclature

Abbreviations

STM	60 mm thickness model
ETM	80 mm thickness model
HTM	100 mm thickness model

Symbols

a_w	Water activity
c	Mass concentrations, $\text{kg}\cdot\text{m}^{-3}$
c_p	Heat capacity, $\text{J}\cdot\text{kg}^{-1}\text{K}^{-1}$
D	Diffusivity, m^2s^{-1}
h_{la}	Latent heat, $\text{J}\cdot\text{kg}^{-1}$
h_T	Heat transfer coefficient, $\text{W}\cdot\text{m}^{-2}\text{K}^{-1}$
h_m	Mass transfer coefficient, $\text{m}\cdot\text{s}^{-1}$
k	Turbulent kinetic energy
K_{evap}	Evaporation rate constant, s^{-1}
M	Molecular weight, $\text{kg}\cdot\text{mol}^{-1}$
M_d	Dry basis moisture content
n	Mass flux, $\text{kg}\cdot\text{m}^{-2}\text{s}^{-1}$
P	Pressure, Pa
R_{const}	Universal gas constant, $\text{J}\cdot\text{mol}^{-1}\text{K}^{-1}$
R_{evap}	Evaporation rate, $\text{kg}\cdot\text{m}^{-3}\text{s}^{-1}$
S	Saturation
T	Temperature, K
\vec{u}	Velocity, $\text{m}\cdot\text{s}^{-1}$
ΔV	Representative elementary volume

Greek symbols

ε	Turbulent dissipation
λ	Thermal conductivity, $\text{W}\cdot\text{m}^{-1}\text{K}^{-1}$
κ	Permeability, m^2
μ	Dynamic viscosity, $\text{Pa}\cdot\text{s}^{-1}$
ρ	Density, $\text{kg}\cdot\text{m}^{-3}$
ω	Mass fraction of air or vapor in gas phase
φ	Porosity
χ	Volume fraction of air or vapor

Subscripts

0	Initial
a	Air
amb	Ambient
cap	Capillary
eff	Effective
g	Gas phase
i	Intrinsic
ir	Irreducible
r	Relative
s	Solid
sat	Saturated
$surf$	Surface
v	Vapor
va	Vapor in air
w	Liquid water

References

1. Ye, J.; Yan, J.; Zhang, Z.; Yang, Z.; Liu, X.; Zhou, H.; Wang, G.; Hao, H.; Ma, K.; Ma, Y.; et al. The effects of threshing and redrying on bacterial communities that inhabit the surface of tobacco leaves. *Appl. Microbiol. Biotechnol.* **2017**, *101*, 4279–4287. [[CrossRef](#)] [[PubMed](#)]
2. Jiang, W.; Wang, L.; Tang, J.; Yin, Y.; Zhang, H.; Jia, T.; Qin, J.; Wang, H.; Wei, Q. Calibration and experimental validation of contact parameters in a discrete element model for tobacco strips. *Processes* **2022**, *10*, 998. [[CrossRef](#)]

3. Wang, W.; Feng, X.; Fan, Z.; Ma, Y.; Chen, X.H.; Ren, Z. Design and application of control strategy for moisture content in redried tobacco strips packed in cases. *Tob. Sci. Technol.* **2020**, *53*, 103–107+112.
4. Zong, J.; He, X.; Lin, Z.; Hu, M.; Xu, A.; Chen, Y.; Zhao, G.; Hu, B.; Jin, Y.; Zou, C. Effect of two drying methods on chemical transformations in flue-cured tobacco. *Dry. Technol.* **2022**, *40*, 188–196. [[CrossRef](#)]
5. Guo, G.-F.; Li, B.; Liu, C.-X.; Jin, X.; Wang, Z.-G.; Ding, M.-Z.; Chen, L.-Y.; Zhang, M.-J.; Zhu, W.-K.; Han, L.-F. Characterization of moisture mobility and diffusion in fresh tobacco leaves during drying by the TG-NMR analysis. *J. Therm. Anal. Calorim.* **2019**, *135*, 2419–2427. [[CrossRef](#)]
6. Janevski, J.; Stojanović, B.; Vukić, M.; Živković, P.; Jovanović, D.D.; Mitrović, D. Experimental investigation of burley tobacco drying process. *Proc. Int. Congr. Process Eng.-Process.* **2019**, *32*, 275–280.
7. Kiranoudis, C.T.; Maroulis, Z.B.; Marinou-Kouris, D. Mass transfer modeling for Virginia tobacco curing. *Dry. Technol.* **1990**, *8*, 351–366. [[CrossRef](#)]
8. Dai, J.-A.; Diao, Y.F. Numerical analysis of transient coupled heat and moisture transfer in textile drying with porous relative impact jet. *Appl. Therm. Eng.* **2022**, *212*, 118613. [[CrossRef](#)]
9. Legros, R.; Millington, C.A.; Clift, R. Drying of tobacco particles in a mobilised bed. *Dry. Technol.* **1994**, *12*, 517–543. [[CrossRef](#)]
10. Pakowski, Z.; Druzdzel, A.; Drwiega, J. Validation of a model of an expanding superheated steam flash dryer for cut tobacco based on processing data. *Dry. Technol.* **2004**, *22*, 45–57. [[CrossRef](#)]
11. Li, C.; Chen, Y.; Zhang, X.; Mozafari, G.; Fang, Z.; Cao, Y.; Li, C. Exergy analysis and optimisation of an industrial-scale circulation counter-flow paddy drying process. *Energy* **2022**, *251*, 123901. [[CrossRef](#)]
12. Bao, Y.; Wang, Y. Thermal and moisture analysis for tobacco leaf flue-curing with heat pump technology. *Procedia Eng.* **2016**, *146*, 481–493. [[CrossRef](#)]
13. Zhang, J.W.; Xin, Y.N.; Li, B. Effects of Temperature and Humidity of Drying Medium on Drying Kinetics of Strips. *Tob. Sci. Technol.* **2014**, *10*, 15–19.
14. Huang, F.; Chen, Q.; Wang, L.; Dou, J.Y.; Wang, S.H.; Li, B. Study on thin-layer dynamic models of humidifying and drying of tobacco strips. *Acta Tabac Sin.* **2014**, *20*, 34–40.
15. Bai, Z.; Guo, D.; Li, S.; Hu, Y. Analysis of temperature and humidity field in a new bulk tobacco curing barn based on CFD. *Sensors* **2017**, *17*, 279. [[CrossRef](#)]
16. Zhu, W.K.; Wang, L.; Duan, K.; Chen, L.Y.; Li, B. Experimental and numerical investigation of the heat and mass transfer for cut tobacco during two-stage convective drying. *Dry. Technol.* **2015**, *33*, 907–914. [[CrossRef](#)]
17. Xin, Y.N.; Zhang, J.W.; Li, B. Drying kinetics of tobacco strips at different air temperatures and relative humidities. *J. Therm. Anal. Calorim.* **2018**, *132*, 1347–1358. [[CrossRef](#)]
18. Zhu, Y.; Wang, P.; Sun, D.; Qu, Z.; Yu, B. Multiphase porous media model with thermo-hydro and mechanical bidirectional coupling for food convective drying. *Int. J. Heat Mass Transf.* **2021**, *175*, 121356. [[CrossRef](#)]
19. Kumar, C.; Joardder, M.U.; Farrell, T.W.; Millar, G.J.; Karim, A. A porous media transport model for apple drying. *Biosyst. Eng.* **2018**, *176*, 12–25. [[CrossRef](#)]
20. Bezerra, C.V.; da Silva, L.H.; Corrêa, D.F.; Rodrigues, A.M. A modeling study for moisture diffusivities and moisture transfer coefficients in drying of passion fruit peel. *Int. J. Heat Mass Transf.* **2015**, *85*, 750–755. [[CrossRef](#)]
21. Wei, S.; Wang, Z.; Wang, F.; Xie, W.; Chen, P.; Yang, D. Simulation and experimental studies of heat and mass transfer in corn kernel during hot air drying. *Food Bioprod. Process.* **2019**, *117*, 360–372. [[CrossRef](#)]
22. Shen, L.; Zhu, Y.; Liu, C.; Wang, L.; Liu, H.; Kamruzzaman, M.; Liu, C.; Zhang, Y.; Zheng, X. Modelling of moving drying process and analysis of drying characteristics for germinated brown rice under continuous microwave drying. *Biosyst. Eng.* **2020**, *195*, 64–88. [[CrossRef](#)]
23. Pletcher, R.H.; Tannehill, J.C.; Anderson, D. *Computational Fluid Mechanics and Heat Transfer*, 3rd ed.; CRC Press: Boca Raton, FL, USA, 2012; ISBN 978-1-4665-7830-2.
24. Wilcox, D.C. *Turbulence Modeling for CFD*, 3rd ed.; DCW Industries: La Canada, CA, USA, 2006; ISBN 978-1-928729-08-2.
25. Joardder, M.U.; Akram, W.; Karim, A. *Heat and Mass Transfer Modelling during Drying: Empirical to Multiscale Approaches*; CRC Press: Boca Raton, FL, USA, 2021; ISBN 978-0-429-46104-0.
26. Ni, H. *Multiphase Moisture Transport in Porous Media under Intensive Microwave Heating*; Cornell University: Ithaca, NY, USA, 1997.
27. Tsilingiris, P.T. Thermophysical and transport properties of humid air at temperature range between 0 and 100 °C. *Energy Convers. Manag.* **2008**, *49*, 1098–1110. [[CrossRef](#)]
28. Halder, A.; Datta, A.K. Surface heat and mass transfer coefficients for multiphase porous media transport models with rapid evaporation. *Food Bioprod. Process.* **2012**, *90*, 475–490. [[CrossRef](#)]
29. Datta, A.K. Porous media approaches to studying simultaneous heat and mass transfer in food processes. II: Property data and representative results. *J. Food Eng.* **2007**, *80*, 96–110. [[CrossRef](#)]
30. Halder, A.; Dhall, A.; Datta, A.K. Modeling transport in porous media with phase change: Applications to food processing. *J. Heat Transf.* **2011**, *133*, 031010. [[CrossRef](#)]
31. Bejan, A. *Convection Heat Transfer*, 4th ed.; John Wiley & sons: Hoboken, NJ, USA, 2013; ISBN 978-0-470-90037-6.
32. Cengel, Y.A.; Boles, M.A. *Thermodynamics: An Engineering Approach*, 8th ed.; McGraw-Hill Education: New York, NY, USA, 2009; ISBN 978-0-07-339817-4.

-
33. Sun, J.; Chen, Y.; Liu, L.; Zhu, F.; Li, Z.; Yu, L.; Xu, S.; Yue, Y.; Ma, Y.; Li, D. Simultaneous Measurement of Temperature-Dependent Thermal Conductivity and Heat Capacity of an Individual Cured Tobacco Leaf. *Int. J. Thermophys.* **2021**, *42*, 132. [[CrossRef](#)]
 34. Pan, D. *Research and Design of Key Technologies for Automatic Tobacco Sorting*; Guizhou University: Guizhou, China, 2016.
 35. Li, X.L.; Hou, P.J.; Li, Q.; Li, H.; Chen, Z.Y.; Zhang, J.S. Differential research on pore structure of different types of tobacco. In Proceedings of the Guangxi Tobacco Society 2018 Paper Collection, Nanning, China, 1 October 2018; pp. 63–70.